Damping Behavior Analysis for Connected Automated Vehicles with Linear Car Following Control

Pengcheng Wang[a], Xiaozheng He[b], Yu Wei [b], Xinkai Wu[c*], Yunpeng Wang [c]

[a] *School of Cyber Science and Technology, Beihang University, Beijing, 100191, China*

[b] *Department of Civil and Environmental Engineering, Rensselaer Polytechnic Institute, Troy, NY 12180, United States*

[c] *School of Transportation Science and Engineering, Beihang University, Beijing, 100191, China*

Abstract: Connected automated vehicles (CAVs), built upon advanced vehicle control and communication technology, can improve traffic throughput, safety, and energy efficiency. Previous studies on CAVs control focus on instability and stability properties of CAV platoons; however, these analyses cannot reveal the damping platoon oscillation characteristics, which are important for enhancing CAV platoon reliability against variant continuous perturbations. To this end, this research seeks to characterize the damping oscillations of CAVs through exploiting the platoon's unforced oscillatory, *i.e.*, *damping* behavior. Inspired by the mechanical vibration theory, this research proposes an approach to analyze the platoon oscillation characterization by formulating the oscillatory dynamics as vibrations in a mechanical system. The proposed approach is applied to a CAV platoon with the linear car-following behavior formulated as Helly's model and the predecessor-following communication topology. Numerical analysis results show that a periodic perturbation with the resonance frequency of the CAV platoon will amplify the oscillation and lead to the severest oscillatory traffic. Our analysis highlights the importance of preventing platoon oscillations from resonance in ensuring CAV platooning reliability.

Keywords: Connected automated vehicles, Damping, Traffic oscillation, Platoon instability, Mechanical vibration theory

[*]Corresponding author.
E-mail address: xinkaiwu@buaa.edu.cn (X. Wu).

1. Introduction

Connected automated vehicles (CAVs) are expected to improve traffic mobility, safety, and sustainability through vehicle automation and connectivity technologies (Shladover, 2018). These technologies enable vehicles to share information through communications to improve travel safety and comfort (Dong *et al.*, 2021), increase traffic capacity (Papadoulis *et al.*, 2019) and reduce pollution (Saxena *et al.*, 2019). To achieve such goals, it is critical for individual CAVs to coordinate with their neighboring vehicles while maintaining stable and safe travel. Therefore, analyzing CAV traffic behavior is of great importance (Jia and Ngoduy, 2016).

Among the research on CAV traffic behaviors, stability, instability, and oscillation are attracting more and more attention. For example, some research investigated the vehicle platoon performance, such as *local stability* and *string stability* (Ding *et al.*, 2020; Zhou *et al.*, 2020). Note that *local stability* is usually used to describe a single vehicle's movement over time under the influence of a small disturbance, *e.g.,* deviation from uniform space gap, velocity, or acceleration; while *string stability* is used to describe how the disturbance is decayed over a vehicle platoon (Sun *et al.*, 2018). In contrast to stability-focused studies, other research aims to investigate instability (Daganzo *et al.*, 2011). The objective of instability analysis is to understand how badly the system could perform. The string instability describes whether the perturbation on the first vehicle will be amplified through the vehicle platoon (Herman *et al.*, 2015). However, neither stability nor instability analysis is sufficient to characterize the damping oscillations of a vehicle platoon. The reason is that string stability (or instability) means that a perturbation imposed on the leader is decayed (or amplified) over the vehicle platoon. However, the damping oscillatory behavior is one of the natural characteristics of the vehicle platoon, which is independent of the imposed perturbation.

Focusing on the damping oscillations of the CAV platoon, this paper introduces a method to characterize the damping oscillations of the vehicle platoon, which is inspired by the mechanical vibration in a spring-mass system. To analyze the performance of a CAV platoon exposed to ubiquitous perturbations, this research exploits the CAV platoon's damping behavior (*i.e.*, unforced oscillatory) by formulating platoon oscillations as vibrations in a mechanical system. To facilitate theoretical derivations, this research employs Helly's model (Helly, 1959) to describe linear car-following dynamics and adopts the predecessor-following (PF) communication scheme to capture the potential perturbations from communications. Upon Helly's model, this paper derives the damping characteristics of the CAV platoon based on the mechanical vibration theory.

Furthermore, this study differentiates damping-based oscillation analysis from existing stability/instability analyses and proposes a new approach to reveal the damping characteristics of CAV platoons using the mechanical vibration theory. The resonance frequency of a CAV platoon, derived based on its damping characteristics, is shown as a function of vehicle control parameters, enabling a quick evaluation involving both the CAV platoon's stability and its damping behavior under perturbation. The analytical characterization of damping behavior, supported by simulation results, shows that a CAV platoon is most vulnerable to periodic perturbations with the same frequency as its inherent fluctuation frequency, also known as *resonance*. Overall, the oscillation analysis of the CAV platoon conveys the insight that preventing perturbations from resonance is crucial to enhance the CAV platooning reliability and suppress large amplitude oscillations.

This study is organized as follows. Section 2 presents the related work about (in)stability and oscillation analysis. Section 3 proposes the oscillation analysis approach to reveal the damping characteristics. Section 4 carries out a simulation study to verify the effectiveness of the proposed method and compare the platoon's oscillations to its stability properties. The last section concludes our findings and suggests future research directions.

2. Related Work

Stability could provide insights into the parametric influence on traveling safety and oscillation propagation. Extensive studies have conducted analyses on CAV stability. For example, Naus *et al.* (Naus *et al.*, 2010) analyzed the string stability of a CAV platoon via a frequency domain approach. Xiao and Gao (Xiao and Gao, 2011) studied the string stability of homogeneous and heterogeneous platoons for vehicles equipped with adaptive cruise control. Ngoduy (Ngoduy, 2013) analyzed the string stability of vehicles equipped with cooperative adaptive cruise control using linear and nonlinear stability methods. Zhou *et al.* (Zhou *et al.*, 2019) presented a predictive control strategy for CAVs and analyzed platoon's local stability and string stability. Ding *et al.* (Ding *et al.*, 2020) pointed out that local stability and string stability are necessary to ensure the performance reliability of the controller and the platoon. Zhou *et al.* (Zhou *et al.*, 2020) formulated a H_∞ control to synthesize control parameters for a mixed vehicular platoon that consists of CAVs and human-driven vehicles and derived a string stability criterion for the mixed vehicular platoon. Herman *et al.* ((Herman *et al.*, 2015) investigated harmonic stability of the platoon, which is a term for exponential scaling of the H_∞ norm of the transfer function of the platoon as the number of the platooned vehicles

increases.

Note that various types of stability have been explored, such as local/asymptotic stability (Chandler *et al.*, 1958; Herman *et al.*, 1959), platoon stability (Wilson and Ward, 2011), and string stability (Swaroop and Hedrick, 1996). To avoid ambiguity, the name 'platoon stability' is also called 'local stability' (Montanino and Punzo, 2021), and 'asymptotic stability' in traffic flow modeling is also called 'string stability' (Ploeg *et al.*, 2014; Qin and Li, 2020). In addition, there exist various stability analysis methods, such as H_∞ norm of the transfer function, leading to various stability conditions. More detailed stability analysis methods and their corresponding stability conditions are presented in (Wilson and Ward, 2011)(Montanino and Punzo, 2021).

By contrast, instability has been widely used to investigate traffic performance under ubiquitous perturbations (Jiang *et al.*, 2018). For example, Montanino and Punzo (Montanino and Punzo, 2021) found that the degree of string instability is higher in a homogeneous platoon than in a heterogeneous one. Treiber and Kesting (Treiber and Kesting, 2018) proposed a generic instability analysis mechanism by introducing white acceleration noise. Jiang *et al.* (Jiang *et al.*, 2018) conducted an experiment to analyze traffic flow instability based on a platoon consisting of 51 vehicles.

Besides stability and instability, traffic/platoon oscillation is another important performance to study CAV traffic behaviors. When traffic/platoon oscillation occurs, vehicles exhibit repetitive deceleration and acceleration operations owing to interactions between slow-moving and fast-moving vehicles. Negative effects of oscillations include driving discomfort, delay, pollution, excessive energy consumption, and increased risk of accident (Li *et al.*, 2010). Meanwhile, such oscillations can easily be triggered by a local perturbation such as lane-changing operations near a bottleneck (Ahn and Cassidy, 2007), cyberattacks on vehicles (Wang *et al.*, 2020), and the abrupt acceleration/deceleration of the human driver or the CAV control system.

Acknowledging the similarity between vehicle platoon oscillation and mechanical vibration of the spring-mass system, researchers have introduced the mechanical vibration theory to modeling and analyzing car-following behaviors. For example, Yanakiev and Kanellakopoulos (Yanakiev and Kanellakopoulos, 1996) employed a simple spring-mass-damper system to capture the longitudinal control of vehicles' behaviors and analyzed the string stability of the vehicle platoon. Li *et al.* (Li *et al.*, 2017) designed a novel car-following model derived from the fundamental physical law of the spring-mass system. They analyzed the stability of the proposed model, in which the quotient of the spring constant and mass represents the sensitivity

coefficient in their proposed car-following model. Munigety *et al.* (Munigety, 2018) proposed a car-following model to describe the longitudinal behaviors of vehicles by using the spring-mass-damper mechanical system. Horn and Wang (Horn and Wang, 2018) applied the spring-mass system to design a bilateral control model of a vehicle platoon. Bang and Ahn (Bang and Ahn, 2020) adopted the spring-mass-damper system to formulate CAVs' behaviors. Furthermore, Li *et al*. (Li *et al.*, 2020) proposed a car-following model that captures the ego vehicle's resistance to large variations in relative speed and special gap when following the preceding vehicle. Unfortunately, all these mentioned studies focus on applying the spring-mass system to formulate car-following behaviors rather than analyzing the vulnerability of vehicle platoon.

However, most of existing studies focus on analyzing the system's (in)stability, and less effort has been conducted on interpreting the damping behaviors. In this study, the damping behavior analysis exploits the platoon's unforced oscillatory dynamics and reveals the inherent oscillation frequency and the damping intensity of the vehicle platoon system, which are important for enhancing CAV platoon reliability against variant continuous perturbations.

3. Damping behavior Oscillation Analysis

This section first discusses the similarity between the mechanical vibration and the vehicle oscillation and presents basic fundaments of the mechanical vibration, then proposes an approach to uncover damping oscillation characteristics and further explore the difference between the proposed damping-based oscillation analysis and classical string stability analysis. The derivation of the damping oscillation characteristics is based on the mechanical vibration theory (Shabana, 2019).

3.1 Preliminaries

This section illustrates the similarity between a vehicular platoon oscillation behavior and the mechanical vibration (*e.g.*, a spring-mass-damper system). Figure 1a shows that, if one person exerts an external force on an object and stretches or contracts the spring away from the equilibrium location, the object will vibrate back and forth around its unstretched location once removing the external force. Due to the damping force, the vibration eventually stops.

Similar to mechanical vibration, Figure 1b presents a vehicular platoon's oscillation behavior. Specifically, if the space gap between two consecutive vehicles is too large, the follower will accelerate to shrink the space gap; otherwise, the follower will decelerate to increase the space gap. The reduplicative acceleration/deceleration makes the vehicles' dynamics unstable and

induces stop-and-go waves. Due to the continuous adjustment of the vehicular control system, the stop-and-go waves gradually die out. The decreasing oscillation magnitude reveals that the vehicle platoon is a damped system, where vehicles dynamics help them achieve the consensus of velocity and space gap.

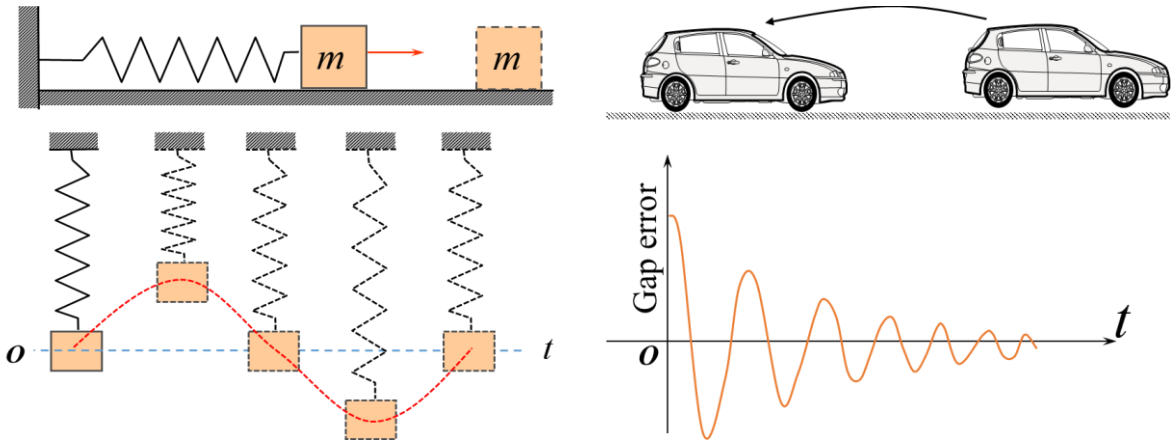

(a) Mechanical variation patterns of an object (b) Platoon oscillation patterns of a vehicle

Figure 1 Schematics of similarities between the mechanical vibration and platoon oscillation

Before we apply the mechanical vibration theory to analyze CAV platoon vulnerability, some major conclusions in mechanical vibration are provided as follows (Kelly, 2012; Schmitz and Smith, 2011).

Consider a system consisting of a rigid mass m and a spring with a recovery constant k. The spring is fixed at one end and attached to the rigid mass at the other end. Suppose that the mass movement is linearly damped by a friction force with coefficient c. The dynamics of this system is modeled by the following second-order differential equation

$$m\ddot{x}(t)+c\dot{x}(t)+kx(t)=0, \tag{1}$$

where $\ddot{x}(t)$, $\dot{x}(t)$ and $x(t)$ are the acceleration, velocity, and position of the mass at time t.

Dividing Eq. (1) by the mass m leads to

$$\ddot{x}(t)+\frac{c}{m}\dot{x}(t)+\frac{k}{m}x(t)=0. \tag{2}$$

Denote $\omega_0=\sqrt{k/m}$ and $\xi=c/2\sqrt{km}$, and substitute them into Eq. (2). Eq. (2) is then rewritten as

$$\ddot{x}(t)+2\xi\omega_0\dot{x}(t)+\omega_0^2x(t)=0 \tag{3}$$

Eq. (3) is the standard form of the differential equation for mechanical vibration systems, where ω_0 is the natural frequency of the motion and ξ is a dimensionless parameter and also called the damping ratio.

Because Eq. (3) is a linear, ordinary homogeneous differential equation with constant coefficients, a solution of Eq. (3) can be assumed to be the form of $x(t) = Ae^{st}$. Substitute it into Eq. (3) leads to

$$\left(s^2 + 2\xi\omega_0 s + \omega_0^2\right) Ae^{st} = 0 \tag{4}$$

If $Ae^{st} = 0$, no motion has occurred and this is referred to as the trivial solution. The characteristic equation is quadratic in s and has two roots, *i.e.*,

$$s_{1,2} = \omega_0\left(-\xi \pm \sqrt{\xi^2 - 1}\right) \tag{5}$$

Hence, the total solution for the system vibration is the sum of the two harmonic responses defined by the two roots, *i.e.*,

$$x(t) = X_1 e^{s_1 t} + X_2 e^{s_2 t} = e^{-\omega_0 \xi}\left(X_1 e^{\omega_0\sqrt{\xi^2-1}} + X_2 e^{-\omega_0\sqrt{\xi^2-1}}\right). \tag{6}$$

In Eq. (6), the first term in the product (*i.e.*, $e^{-\omega_0\xi}$) describes the damping envelope that bounds the decaying oscillation and the second term (*i.e.*, $X_1 e^{\omega_0\sqrt{\xi^2-1}} + X_2 e^{-\omega_0\sqrt{\xi^2-1}}$) defines the oscillatory part (Schmitz and Smith, 2011). Owing to Eq. (6), there are three domains for ξ, which lead to different solutions to Eq. (1).

Based on the above preliminaries, we have the following fundamentals of the mechanical vibration theory.

Definition 1 (Natural frequency). Natural frequency is the frequency at which a system tends to oscillate in the absence of any driving or damping force.

Definition 2 (Resonance freqeuncey). Resonance frequency is identified where the forcing frequency is equal to or close to the natural frequency, which could lead to the largest vibration amplitude.

Remark 1. The mechanical vibration system Eq. (1) is the general form of the differential equation for the displacement of an object in a linear system with viscous damping. Based on Eq. (6), different solutions of this equation have different vibration characteristics (Kelly, 2012):

1) If $\xi > 1$, the roots of Eq. (1) are real, it is called the overdamped system. In this case, the motion of this system is nonoscillatory.

2) If ξ=1, the roots of Eq. (1) are equal, it is called the critically damped system. In this case, the motion of this system is also nonoscillatory.

3) If ξ<1, the roots of Eq. (1) are complex conjugates, it is called the underdamped system. In this case, the motion of this system is oscillatory.

Note that the complex roots of Eq. (1) will introduce the oscillatory component. Any complex number can be written in exponential form $z = re^{i\theta}$. A time-dependent complex number can be denoted as $z(t) = re^{i\omega t} = r\cos\omega t + ir\sin\omega t$ (Hahn, 1994). At time t, $z(t)$ is at a point on the circle of radius r at angle ωt to the *x*-axis. Namely, $z(t)$ is circling at a steady angular velocity ω, i.e., $z(t) = re^{i\omega t} = r\cos\omega t + ir\sin\omega t$. These trigonometric functions can be used to describe harmonic oscillations, because harmonic oscillations can be regarded as the projection of the circling complex number on a straight line (Schmitz and Smith, 2011). In the context of a CAV platoon, the communication between two vehicles can be regarded as a spring between them. Then the object's acceleration $\ddot{x}(t)$, velocity $\dot{x}(t)$, and position $x(t)$ are similar to the CAV's acceleration, velocity, and position. The following will apply the mechanical vibration theory to derive the CAV's damped oscillation characteristics.

3.2 Analysis approach

This section aims to derive the damping oscillation characteristics of a CAV platoon by using the mechanical vibration theory. As discussed above, the process of the oscillation amplitude decay is similar to the mechanical vibration of the spring-mass system. Therefore, based on this similarity, we will apply the vibration theory, *i.e.*, Definitions 1 and 2 and results in Remark 1, to investigate the damping oscillation characteristics of the platoon system.

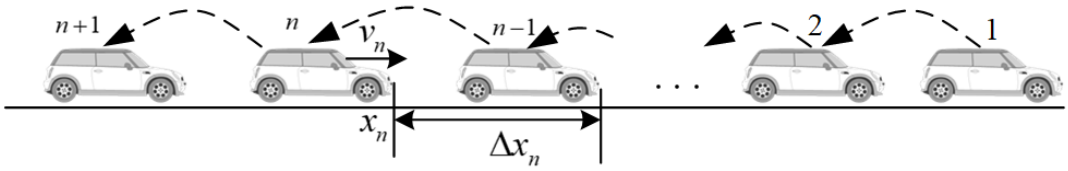

Figure 2 Illustration of the platooned vehicles on a single lane

In our theoretical derivation, we consider a platoon of homogeneous CAVs moving on a single lane, as depicted in Figure 2, where x_n represents the position of vehicle n, v_n represents the speed of vehicle n, and $\Delta x_n = x_{n-1} - x_n$ represents the space headway or distance between vehicle n and vehicle $n-1$. To capture the vehicle's longitudinal dynamics, a car-following model is formulated as follows:

$$\begin{aligned} \dot{x}_n &= v_n(t), \\ \dot{v}(t) &= f\left(s_n, v_n, \Delta v_n\right). \end{aligned} \tag{7}$$

where $s_n = x_{n-1} - x_n - l_{n-1}$ represents the space gap between vehicle n and vehicle $n-1$ with l_{n-1} indicating the length of vehicle $n-1$, and $\Delta v_n = v_n - v_{n-1}$ represents the relative velocity between vehicle n and vehicle $n-1$.

For any vehicle $n \in \{1, \cdots, m\}$, a perturbation to vehicle n could affect v_n, x_n and s_n. These changes can be expressed as deviations μ_n and y_n from the equilibrium values v^{e}, s^{e}, *i.e.*:

$$\begin{aligned} v_n(t) &= v^{\mathrm{e}}(t) + \mu_n(t), \\ s_n(t) &= s^{\mathrm{e}}(t) + y_n(t), \end{aligned} \tag{8}$$

where $y_n(t) = x_{n-1}(t) - x_n(t) - l_{n-1} - s^{\mathrm{e}}(t)$ and $\mu_n(t) = v_n(t) - v^{\mathrm{e}}(t)$.

When a change in the gap and/or velocity occurs on vehicle n, in this time, the velocity of vehicle $n-1$ keeps its steady velocity and is a constant, and s^{e} is also a constant. Based on Eq. (8), we can derive

$$\frac{\mathrm{d}y_n(t)}{\mathrm{d}t} = \frac{\mathrm{d}x_{n-1}(t)}{\mathrm{d}t} - \frac{\mathrm{d}x_n(t)}{\mathrm{d}t} = v^e(t) - v_n(t) = -\mu_n(t). \tag{9}$$

Hence, based on Eqs. (7) and (9), we can derive the following equations.

$$\begin{aligned} \frac{\mathrm{d}y_n}{dt} &= -\mu_n, \\ \frac{\mathrm{d}\mu_n}{\mathrm{d}t} &= f\left(s^e + y_n, v^e + \mu_n, \mu_n\right). \end{aligned} \tag{10}$$

By employing the first-order Taylor expansion to Eq. (10), we can find that

$$\frac{\mathrm{d}\mu_n}{\mathrm{d}t} = f_n^v \mu_n + f_n^s y_n + f_n^{\Delta v} \mu_n + o(\mu_n, y_n). \tag{11}$$

Ignoring the high-order terms in Eq. (11), the linear part can be written as:

$$\frac{\mathrm{d}^2 y_n}{dt^2} - \left(f_n^v + f_n^{\Delta v}\right)\frac{\mathrm{d}y_n}{dt} + f_n^s y_n = 0. \tag{12}$$

Defining $-\left(f_n^v + f_n^{\Delta v}\right) = 2\omega_0 \xi$ and $f_n^s = \omega_0^2$, Eq. (12) can be rewritten as

$$\frac{d^2 y_n}{dt^2} + 2\omega_0 \xi \frac{dy_n}{dt} + \omega_0^2 y_n = 0 \tag{13}$$

where $\xi = -\frac{1}{2}\left(f_n^v + f_n^{\Delta v}\right) \Big/ \sqrt{\left|f_n^s\right|}$ and $\omega_0^2 = f_n^s$.

Note that Eq. (13) is akin to the mechanical vibration system, which is also a general form of the differential equation for the displacement of a particle in a linear system with viscous damping (Thomson, 2018). Herein, referring to **Definition 1**, ω_0 represents an inherent oscillation frequency, at which the system oscillates independently of any external excitation. Furthermore, the inherent oscillation frequency is also called *resonance frequency*. If the

perturbation is exerted on vehicles with the *resonance frequency*, as presented in **Definition 2**, this could lead to the largest vibration amplitude (Shabana, 2019).

Notation ξ in Eq. (6) represents the damping intensity of a system against vibration. In particular, in the field of mechanical vibration, as presented in **Remark 1**, $\xi < 1$ indicates an underdamped system; and $\xi \geq 1$ indicates an overdamped system. Based on the definition of damping dynamics in mechanical vibration, for a vehicle platoon system, $\xi < 1$ represents the scenario that the perturbed platoon oscillates back and forth around the equilibrium state; and $\xi \geq 1$ represents that the perturbed platoon can converge to its equilibrium state without overshoots. Therefore, a platoon control strategy that ensures $\xi \geq 1$ can enable the platoon to resist external perturbation more effectively. Such resistance is helpful in enhancing platoon reliability in a complex travel environment.

3.3 Damping-based oscillation analysis for a platoon with linear following behavior

This study applies the proposed approach to a vehicle dynamics model to illustrate its capability in uncovering a CAV platoon's damping oscillatory behavior. Over the years, a variety of car-following models have been developed, such as Pipes' model, Helly's model, optimal velocity model (OVM), and intelligent driver model (IDM) (Aghabayk *et al.*, 2015). Among them, due to the simple and intuitive features, Helly's linear car-following model has been widely used to describe CAV's behaviors (Chen *et al.*, 2021; Hu *et al.*, 2021). Hence, this study adopts Helly's car-following model to capture the longitudinal acceleration of the CAV. The formulation of this model is expressed as below (Helly, 1959):

$$\dot{v}_n(t) = \lambda_x \left(s_n(t) - \tau v_n(t) - s_0 \right) - \lambda_v \Delta v_n(t), \tag{14}$$

where λ_v represents the sensitivity to relative velocity, λ_x represents the sensitivity to distance difference between two successive vehicles, s_0 is the minimum distance allowed as a safety gap, and τ represents reaction time. Note that $\tau v_n(t) + s_0$ indicates the desired space gap. In this model, the acceleration of a vehicle presents a linear relationship with the deviation from the space gap and the relative velocity between two successive vehicles.

In a steady state, each vehicle maintains an identical space gap and velocity. Therefore, Eq. (14) can be expressed as bellows.

$$s^{\mathrm{e}} = \tau v^{\mathrm{e}} + s_0 \tag{15}$$

where v^{e} and s^{e} represent the steady velocity and steady space gap, respectively.

Furthermore, in addition to Helly's linear model, this study assumes a predecessor-following

communication scheme. In this way, we can better reveal the damping oscillation characteristics of a vehicle platoon. With the predecessor-following communication, each CAV can share its information and receive other vehicles' information. The communication topology defines the origins and destinations of information spreading among CAVs that can affect the vehicle dynamics, thereby playing a critical role in information exchange and sharing. Note that many communication topologies have been proposed for CAV platoons, *e.g.*, predecessor-following, predecessor-leader-following, bidirectional, bidirectional-leader, two-predecessors following, two-predecessor-leader following, multiple-predecessor-following, and multiple-predecessor-leader-following (Wang *et al.*, 2019). However, those complex communication topologies introduce extra difficulties in the analytical derivation of oscillation characteristics, which will divert the focus of this research. To better elucidate our proposed approach to derive closed-form formulas for the damping oscillation characteristics, we assume that the subject vehicle only receives its nearest preceding vehicle.

Hence, based on the derivations of the partial derivatives in Section 3.2, the damping oscillation characteristics of Helly's linear model can be derived, *i.e.*,

$$\omega_0 = \sqrt{\lambda_x}, \quad \text{and} \quad \xi = \frac{1}{2}\left(\sqrt{\lambda_x}\tau + \lambda_v / \sqrt{\lambda_x}\right). \tag{16}$$

Note that the oscillation damping performance analysis could also be applied to the general human-driven vehicle's longitudinal behavior. However, this study pays more attention to perturbations caused by cyberattacks (Wang *et al.*, 2020) and communication information noises (Vegamoor *et al.*, 2021) on the CAV platoon. Such effects are formulated as periodic perturbations in the numerical examples presented in Section 4. Hence, we would like to apply our proposed approach in the CAV context. Furthermore, this study is our first attempt to investigate the damping characterizes of the vehicle platoon system. To articulate the basics, we only adopt a simple linear model, *i.e.*, Helly's model, for theoretical analysis. In fact, our proposed approach can also be applied to high-order models such as the optimal velocity model (OVM) and intelligent driver model (IDM) by using the linearization method (Ngoduy, 2015; Sun *et al.*, 2018). Detailed work on high-order models is still under investigation and will be published in other papers in the future.

3.4 Differences between damping-based oscillation and instability analysis

It is necessary to differentiate the damping-based oscillation and (in)stability. First, through the (in)stability analysis on the linear model, we can obtain the (in)stability condition (Detailed

derivation of the instability analysis are presented in Appendix). The instability condition of Helly's model is shown below.

$$\lambda_v < \frac{1}{\tau} - \frac{\lambda_x \tau}{2}. \tag{17}$$

When a perturbation is exerted on the vehicle platoon, the perturbation effect decays for a stable system; or the perturbation effect grows for an unstable system (Pueboobpaphan and van Arem, 2010). However, such instability analysis focuses on the propagation of the perturbation effect (Yao *et al.*, 2020) and cannot characterize the damping oscillation.

More importantly, from Eqs. (16) and (28), we can visually compare the instability and damping-based oscillation conditions, as shown in Figure 3. In the instability analysis, Figure 3a shows that a curve divides the regions into stable and unstable regions. The area above the curve denotes the stable region, while the area below the curve denotes the unstable region. Figure 3b indicates that the whole plane is divided into underdamped and overdamped regions. The region above the curve is overdamped, and the region below the curve is underdamped regions. These two figures clearly illustrate the difference between instability analysis and damping-based oscillation analysis.

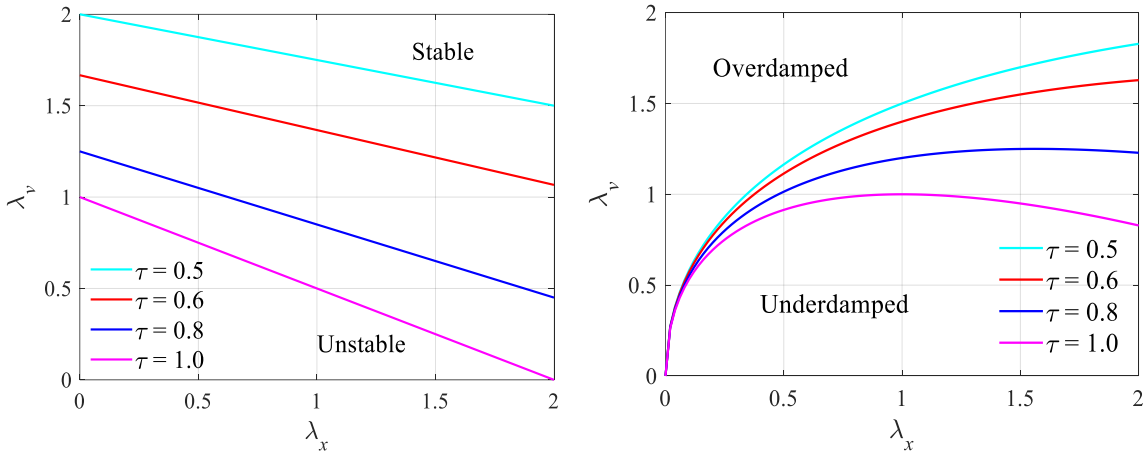

(a) Stable and unstable regions (b) Underdamped and overdamped regions

Figure 3 Instability and damping-based oscillation analysis on a linear model

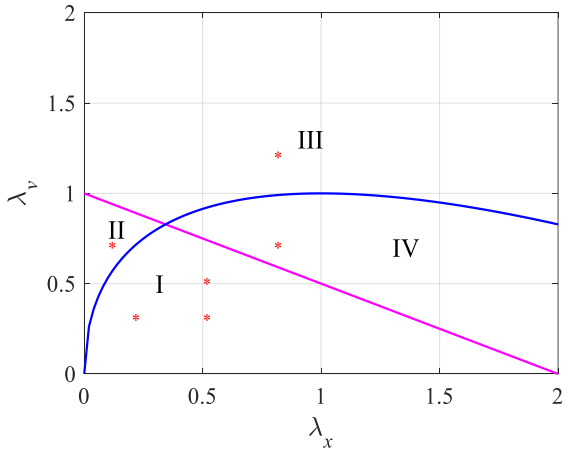

Figure 4 Regions for the instability and damping-based oscillation analysis when $\tau = 1$. The magenta line indicates the boundary of the stable and unstable regions, and the blue curve indicates the boundary of the underdamped and overdamped regions.

The instability boundary line and the damping characteristic curve divide the whole plane into four regions, as shown in Figure 4. In detail, Region I represents the unstable and underdamped region, Region II represents the unstable and overdamped region, Region III represents the stable and overdamped region, and Region IV represents the stable and underdamped region. In this figure, each region has the dual features of stability and damping oscillation. For example, if the parameters λ_x and λ_v are selected from Region I, the vehicle platoon presents unstable and underdamped oscillation properties, which means the perturbation amplifies as it propagates to the vehicle platoon and the oscillations resulting from perturbations present back-and-forth fluctuations around the equilibrium. The oscillation properties of other regions can be described accordingly.

The above analyses help us derive an approach to reveal the damping oscillation characteristics of the vehicle platoon and elucidate the difference between the proposed analysis approach and the existing string (in)stability analysis methods. Overall, the damping process is an inherent property independent of external perturbations exerted on the platoon, meaning that the system has an instinct to resist the oscillation. The damping behavior of a system refers to the characteristic of how a perturbation, when applied to a system, dissipates over time. The damping oscillation properties, including the inherent oscillation frequency and damping intensity, will convey profound knowledge in understanding oscillations and designing effective traffic management strategies to help traffic against various perturbations. Through the proposed approach, we derive two parameters, *i.e.*, the inherent oscillation frequency or called resonance frequency (*i.e.*, ω_0) of the CAV platoon and the damping intensity (*i.e.*, ξ) of the

platoon system against vibration. If the perturbation is exerted on vehicles with the resonance frequency, this could lead to the largest vibration amplitude. The underdamped condition (*i.e.*, $\xi < 1$) represents that the perturbed platoon oscillates back and forth around the equilibrium state; and the overdamped condition (*i.e.*, $\xi \geq 1$) represents that the perturbed platoon can recover back to its equilibrium state without overshoots.

Instead, string stability relates to the characterization of how the perturbation dissipates along a string of vehicles. To demonstrate the differences, we derive the stable or unstable conditions using the classical string stability analysis approach. Stable or unstable conditions mean that a perturbation imposed on the leader is decayed or amplified over the vehicle platoon. As our proposed method focuses on platoon oscillation characterization, it differs from the classical string stability analysis methods. The following section will illustrate the significance of applying our proposed approach to analyze the impact of perturbation on platoon system performance through simulation.

4. Numerical Analysis

A CAV platoon consisting of 10 vehicles and traveling in a single lane is assumed in our numerical analysis. The first leading vehicle remains its initial velocity during the entire simulation that is 100 s. Each vehicle's parameters are set as bellow: the desired free-flow speed $v_0 = 33$ m/s, vehicle length $l = 5$ m, the minimum safety distance $s_0 = 2$ m, the maximum acceleration $a = 5\ \text{m/s}^2$, and the desired deceleration $b = 6\ \text{m/s}^2$ (Milanes and Shladover, 2014; Niroumand *et al.*, 2020). The velocity and position are updated by the following kinematic equation.

$$\begin{aligned} v_n(t+\Delta t) &= v_n(t) + 0.5\big(a_n(t) + a_n(t+\Delta t)\big)\Delta t, \\ x_n(t+\Delta t) &= x_n(t) + v_n(t)\Delta t + 0.5 a_n(t)\big(\Delta t\big)^2. \end{aligned} \tag{18}$$

where Δt is the sampling time step and set as 0.1s.

Note that no overtaking is allowed. If the following vehicle exceeds its preceding vehicle, then a rear-end collision occurs. Next, to verify the theoretical results presented in Section III, we conduct three simulation scenarios on the CAV platoon: without perturbation, with periodic perturbation, and with the human-driven vehicle trajectory. Scenario I is defined as the base case without external perturbation after time 0 and focuses on illustrating how the vehicle platoon behaviors are affected by different values of λ_x and λ_v without external perturbation. Scenario II characterizes the platoon behaviors affected by a periodic perturbation after time 0. Scenario III presents more realistic platoon behaviors impacted by a human-driven vehicle

trajectory. To be consistent with Figure 4, the reaction time, τ, is set as 1s.

4.1 Scenario I: Without perturbation

As Eq. (16) shows, inherent oscillation frequency ω_0 and damping intensity ξ are determined by parameters λ_x, λ_v. Hence, to understand the joint impact of 'damping behavior' and 'stability' behavior, we conduct a multiple experiments, four cases are presented.

(i) Case 1 describes the vehicle platoon behaviors in Region II, whose parameters correspond to three red asterisks in Region I of Figure 3.

(ii) Case 2 describes the vehicle platoon behaviors in Region II, whose parameter corresponds to the red asterisk in Region II of Figure 3.

(iii) Case 3 describes the vehicle platoon behaviors in Region III, whose parameter corresponds to the red asterisk in Region III of Figure 3.

(iv) Case 4 describes the vehicle platoon behaviors in Region IV, whose parameter corresponds to the red asterisk in Region IV of Figure 3.

Case 1: Unstable and underdamped condition in Region I

For consistency, we assume that at the initial stage, each vehicle's speed is 15 m/s, and each vehicle's space gap is set as 10 m. At equilibrium, each vehicle remains the same velocity as the first leading vehicle, *i.e.*, 15 m/s, and each following vehicle has an identical space gap, *i.e.*, the stable space gap is 17 m/s. Indeed, the space gap can also be obtained according to Eq. (15) . In Figure 5, the parameters $\lambda_x = 0.2$ and $\lambda_v = 0.3$ are selected from Region I. Meanwhile, based on Eq. (16), we can derive $\omega_0 = 0.4472$ rad/s and $\xi = 0.5590 < 1$, which indicates the vehicle platoon system is underdamped. As we can see from this figure, the perturbation grows as it propagates to the following vehicles. In other words, the system is said to be unstable.

Figure 6 and Figure 7 show the change of position, velocity, and space gap with time when $\lambda_x = 0.5, \lambda_v = 0.3$ and $\lambda_x = 0.5, \lambda_v = 0.5$, respectively. Using Eq. (16), we can calculate $\omega_0 = 0.7071$ rad/s and $\xi = 0.5657 < 1$ for the case shown in Figure 6 and $\omega_0 = 0.7071$ rad/s and $\xi = 0.7071 < 1$ for the case shown in Figure 7. All these figures show unstable traffic, *i.e.*, the perturbation grows over the vehicle platoon. Among them, we found that with the increase of ξ, the oscillation amplitude of the vehicle platoon turns smaller. This also demonstrates that the damping intensity ξ can be used to describe the system performance, and the larger ξ, the smaller oscillations.

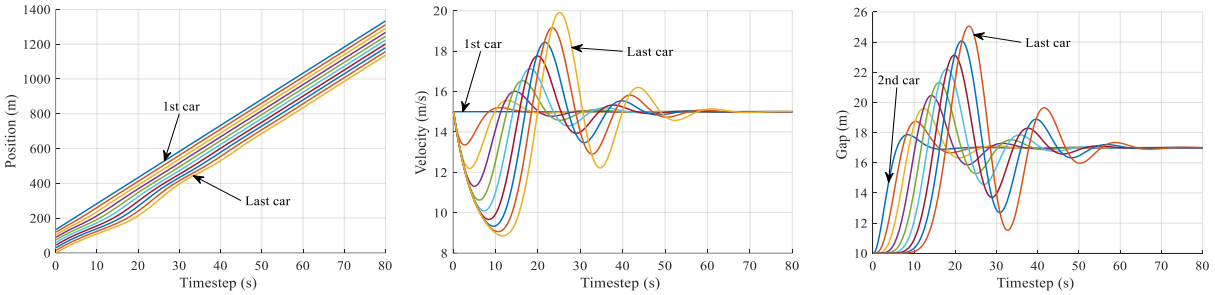

(a) Position vs. time (b) Velocity vs. time (a) Gap vs. time

Figure 5 Unstable and underdamped platoon's position, velocity, and gap evolution when $\lambda_x = 0.2, \lambda_v = 0.3$

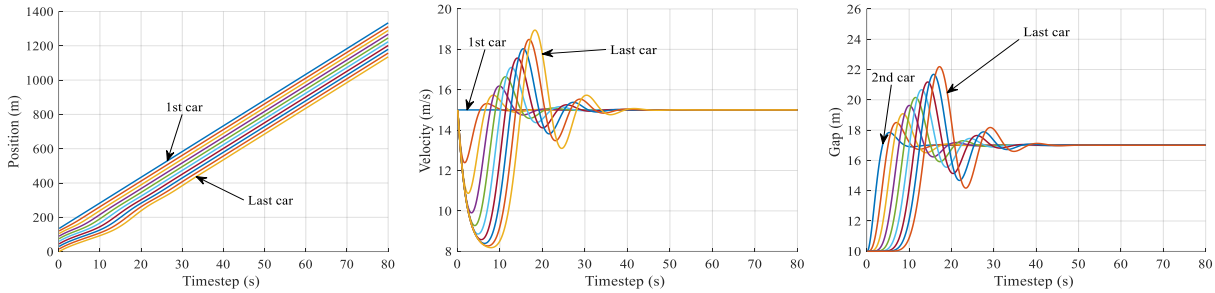

(a) Position vs. time (b) Velocity vs. time (a) Gap vs. time

Figure 6 Unstable and underdamped platoon's position, velocity, and gap evolution when $\lambda_x = 0.5, \lambda_v = 0.3$

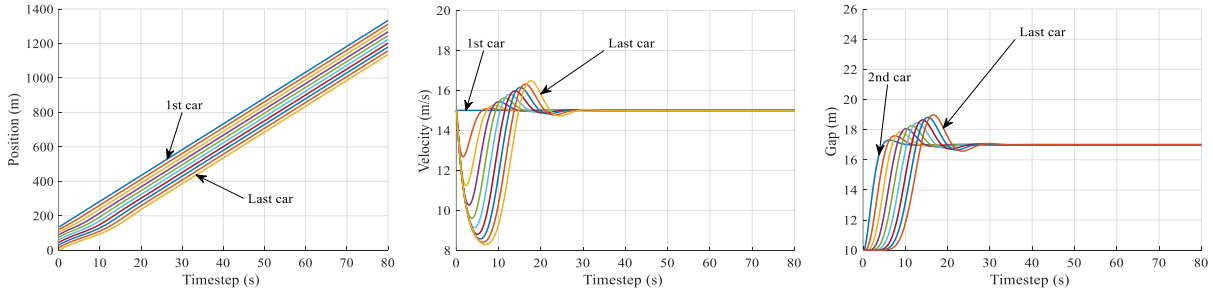

(a) Position vs. time (b) Velocity vs. time (a) Gap vs. time

Figure 7 Unstable and underdamped platoon's position, velocity, and gap evolution when $\lambda_x = 0.5, \lambda_v = 0.5$

Case 2: Unstable and overdamped condition in Region II

In this case, we present the vehicle platoon behaviors under unstable and overdamped conditions. Herein, we select $\lambda_x = 0.1, \lambda_v = 0.6$ which lies in Region II. Herein, $\omega_0 = 0.3162$ rad/s and $\xi = 1.2649 > 1$. When $\xi > 1$, it means the system is overdamped. This case aims to discuss the impact of these parameters on oscillations of the vehicle platoon. Figure 8 shows the evolution of position, velocity, and space gap with time for this case. Compared with Figure 5-7, the vehicle platoon hardly oscillates, and the changes of velocity and gap are relatively small. The reason is that a large ξ yields a strong ability to resist the oscillation. This result is

in accordance with the theoretical result discussed in Section 3, *i.e.*, $\xi \geq 1$ represents that the perturbed platoon can converge to its equilibrium state without overshoots. These figures also show that the oscillation amplitude increases with the length of the vehicle platoon, demonstrating an unstable system.

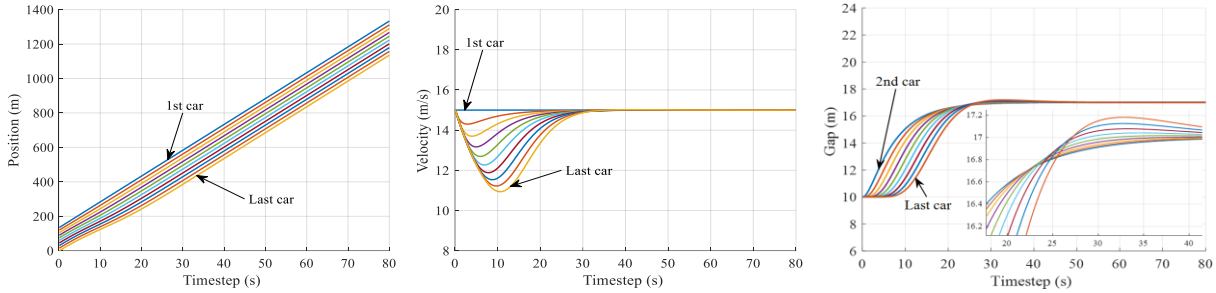

(a) Position vs. time (b) Velocity vs. time (a) Gap vs. time

Figure 8 Stable and overdamped platoon's position, velocity, and gap evolution when

$$\lambda_x = 0.1, \lambda_v = 0.6$$

Case 3: Stable and overdamped condition in Region III

Figure 9 presents the change of position, velocity, and space gap with time when $\lambda_x = 0.8, \lambda_v = 1.2$. At this moment, we can derive that $\omega_0 = 0.8944$ rad/s and $\xi = 1.1180 > 1$, which means that the platoon system is overdamped. Based on Eq. (17), we can calculate that the platoon system is stable. The changes in velocity and spacing gap are relatively smooth. This case shows that the initial perturbation recovers back to its equilibrium state without overshoots. The reason is that the overdamped system hardly oscillates, and for a stale system, the perturbation decays with the vehicle platoon.

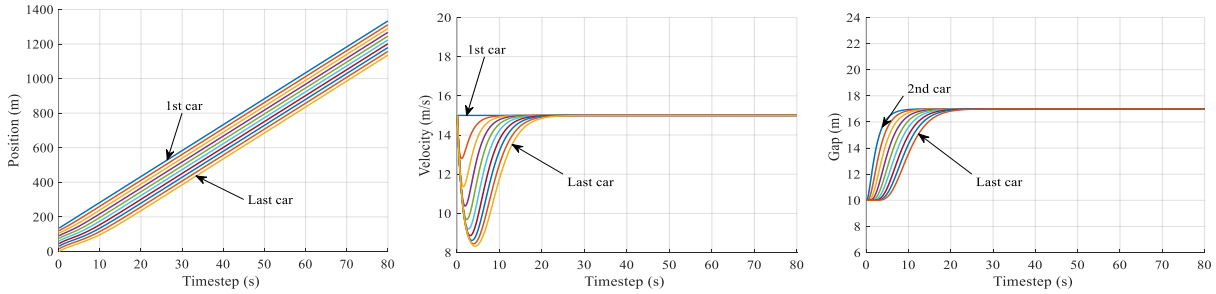

(a) Position vs. time (b) Velocity vs. time (a) Gap vs. time

Figure 9 Stable and overdamped platoon's position, velocity, and gap evolution when

$$\lambda_x = 0.8, \lambda_v = 1.5$$

Case 4: Stable and underdamped condition in Region IV

Figure 10 presents the change of position, velocity, and space gap with time when $\lambda_x = 0.8, \lambda_v = 0.7$. Then we can find that $\omega_0 = 0.8944$ rad/s and $\xi = 0.8385 < 1$, which means the platoon system is underdamped. Based on Eq. (17), we can derive that the platoon system is stable. Similar to Figure 9, the initial unsteady state makes the vehicle platoon return to an

equilibrium state after a string of oscillations of mild amplitudes. The reason is that the larger ξ means the system has a significant ability to resist the oscillation.

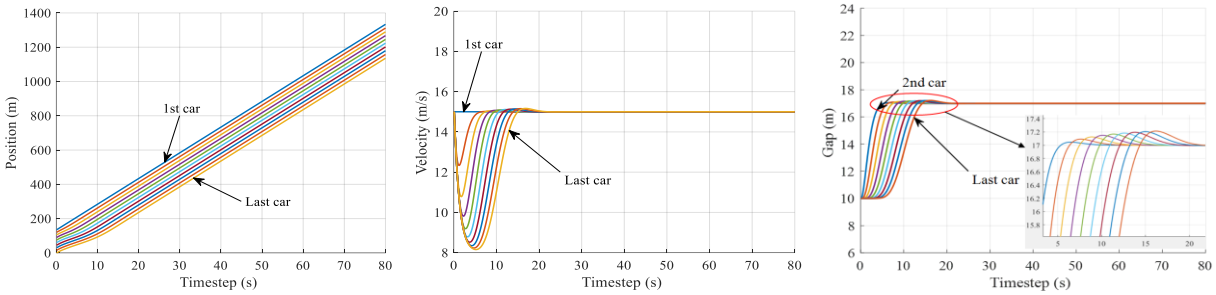

(a) Position vs. time (b) Velocity vs. time (a) Gap vs. time

Figure 10 Stable and underdamped platoon's position, velocity, and gap evolution when $\lambda_x = 0.8, \lambda_v = 0.7$

From the above simulations, we can find that different parameters λ_x, λ_v could determine the oscillation behaviors of the vehicle platoon. For example, the unstable platoon system shows a larger oscillation than the stable system. Furthermore, the perturbation oscillates back and forth in an underdamped system and hardly oscillates in an overdamped system. In addition, we also find that the larger the value of the damping intensity ξ for a platoon system, the smaller the oscillation behaviors of the vehicle platoon. These cases demonstrate that the damping intensity ξ can be regarded as a performance index to evaluate the oscillation amplitude of the vehicle platoon.

4.2 Scenario II: With periodic perturbation

This scenario assumes that a periodic perturbation with specified frequency and amplitude is exerted on the CAV platoon. The purpose of this scenario is twofold. First, it clarifies the different oscillation behaviors with different sets of λ_x, λ_v by comparing with Scenario I. Second, it explores the occurrence and impact of resonance when different periodic perturbations are exerted on vehicles.

Noted that periodic perturbation is a ubiquitous event or process in nature, such as sound, noise, and vibration, occurring on varied spatial and temporal scales, which can immediately influence system stability (Norton and Karczub, 2003). For a vehicle platoon system, such a periodic perturbation may be from the control system's noise (Treiber and Kesting, 2018) or malicious cyberattack (Wang *et al.*, 2020). When stable conditions are satisfied, the perturbations are not amplified. However, under extreme conditions, a small perturbation can amplify vehicle platoon oscillation. If a periodic perturbation is released with different frequencies, then the oscillation pattern of the vehicle platoon changes. Therefore, to capture

abnormal platoon vehicle behaviors, especially to uncover the damping oscillation characteristics of the vehicle platoon, a series of simulations are conducted as follows.

Same as Scenario I, in the steady-state, each vehicle's velocity is 15 m/s, and each following vehicle has an identical space gap, *i.e.*, 17 m. Hence, to exclude the impact of transition from an unstable state to an equilibrium state of the vehicle platoon, the initialized velocity is set as 15 m/s, and the space gap is 17 m. Without loss of generality, we assume the space gap error of the 1st vehicle is disturbed in a sinusoidal fashion, *i.e.*,

$$\begin{aligned} s_n(t) &= s^{\mathrm{e}} + y_n(t) \\ y_n(t) &= Y \sin\left(\omega_f t\right) \end{aligned} \tag{19}$$

Besides, we assume that the perturbation happens at 10 s and ends at 20 s. For comparison, we also present four cases that are consistent with Scenario I. Each case shows the impact of a perturbation with low frequency, resonance frequency, and high frequency on the CAV platoon, *i.e.*, $\omega = 0.2$ rad/s, $\omega = \omega_0$ and ω=1.2 rad/s, respectively, where $Y = 0.6$ m. The perturbation period is indicated by two vertical dashed lines in these figures.

Case 5: Unstable and underdamped condition in Region I

Same as Figure 4, herein, $\lambda_x = 0.2, \lambda_v = 0.3$. As this time, the inherent oscillation frequency ω_0 is 0.4472 rad/s, and the damping intensity ξ is 0.5590<1. Figure 11-13 show the impact of a perturbation with low frequency, resonance frequency, and high frequency on the CAV platoon, *i.e.*, $\omega = 0.2$ rad/s, $\omega = \omega_0 = 0.4472$ rad/s, and ω=1.2 rad/s, respectively. These figures present a larger oscillation amplitude. The reason is that the platoon system is unstable and underdamped. In particular, the oscillation amplifies with the number of vehicles, and the oscillation fluctuates around the equilibrium state. Compared to Figure 11&13, the perturbation with the resonance frequency in Figure 12 causes the most significant oscillation. Furthermore, the perturbation amplitudes of velocity and space gap in Figure 12 are much larger than those in Figure 11 or Figure 13. Moreover, even a rear-end collision happens in Figure 12. Hence, through this case, we found that under the same conditions, the perturbation with the resonance frequency on the vehicle platoon can have serious consequences.

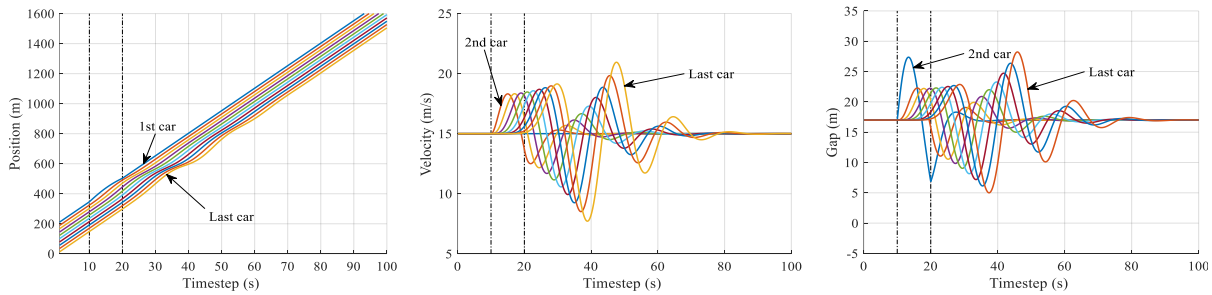

(a) Position vs. time (b) Velocity vs. time (a) Gap vs. time

Figure 11 Unstable and underdamped platoon's position, velocity, and gap evolution under $\omega = 0.2$ rad/s

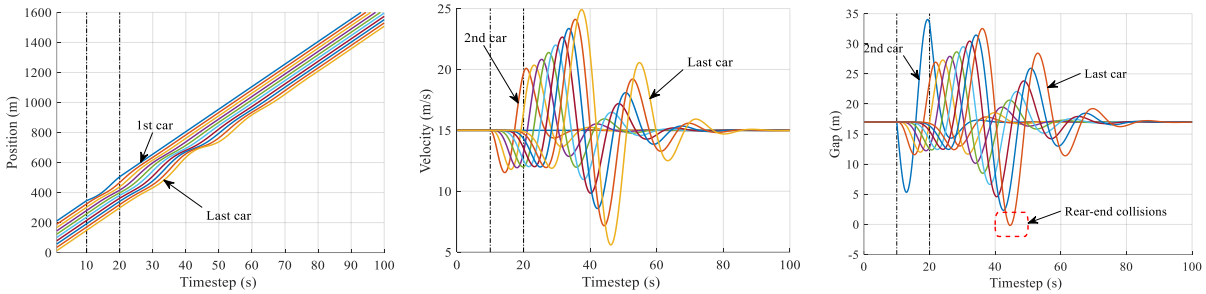

(a) Position vs. time (b) Velocity vs. time (a) Gap vs. time

Figure 12 Unstable and underdamped platoon's position, velocity, and gap evolution under $\omega = \omega_0 = 0.4472$ rad/s

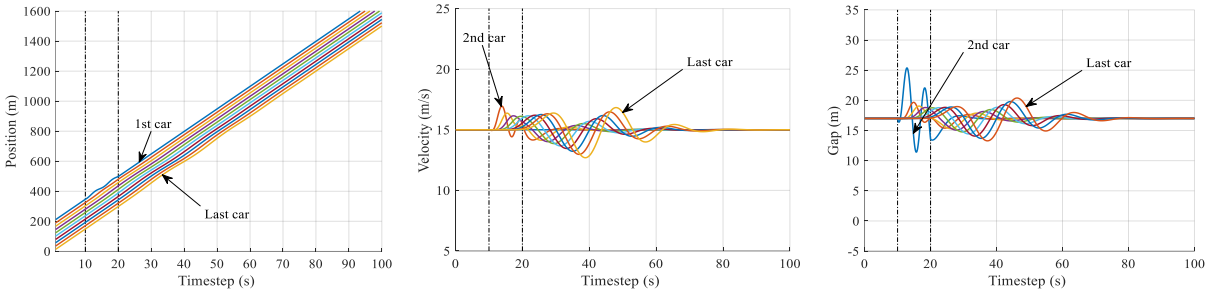

(a) Position vs. time (b) Velocity vs. time (a) Gap vs. time

Figure 13 Unstable and underdamped platoon's position, velocity, and gap evolution under $\omega = 1.2$ rad/s

Case 6: Unstable and overdamped condition in Region II

For the same as Case 2 of Scenario I, herein, we select $\lambda_x = 0.1$ and $\lambda_v = 0.7$, then we can derive $\omega_0 = 0.3162$ and $\xi = 1.2649 > 1$. The vehicle platoon system with the given parameters represents an unstable and overdamped system. Figure 14-16 present the impact of a perturbation with different frequencies on the CAV platoon. These figures present a platoon's dynamics with mild oscillation. Because this system is unstable and overdamped, the oscillation grows with the propagation of the vehicle platoon, and the platoon hardly oscillates. Compared to Figure 14&16, the perturbation with the resonance frequency in Figure 15 causes the largest oscillation. In addition, as shown in Figure 15(c), the perturbation with the resonance frequency results in a rear-end collision.

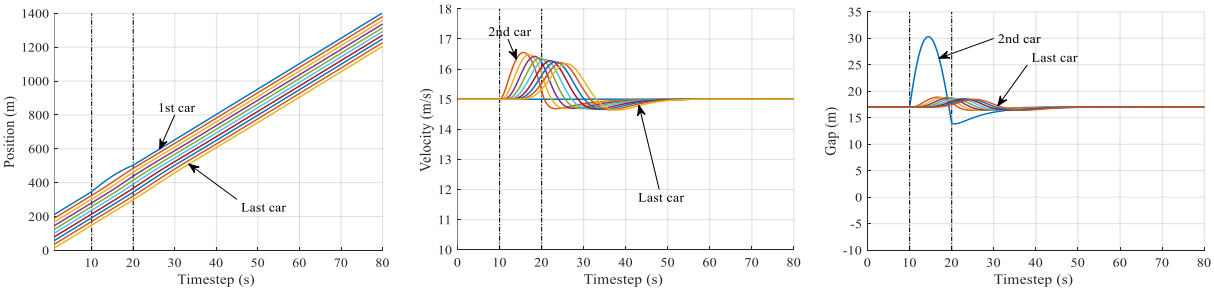

(a) Position vs. time (b) Velocity vs. time (a) Gap vs. time

Figure 14 Unstable and overdamped platoon's position, velocity, and gap evolution under $\omega = 0.2$ rad/s

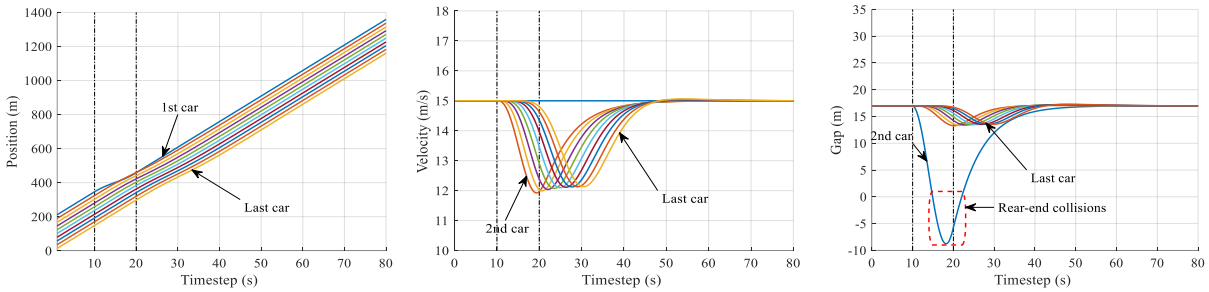

(a) Position vs. time (b) Velocity vs. time (a) Gap vs. time

Figure 15 Unstable and overdamped platoon's position, velocity, and gap evolution under $\omega = \omega_0 = 0.3162$ rad/s

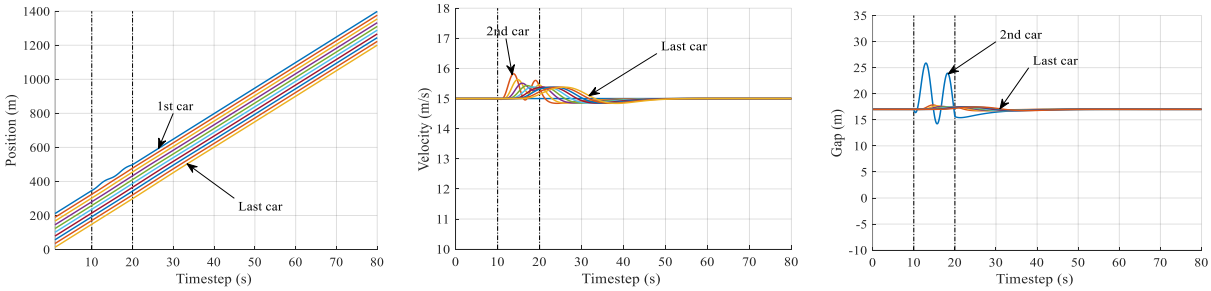

(a) Position vs. time (b) Velocity vs. time (a) Gap vs. time

Figure 16 Unstable and overdamped platoon's position, velocity, and gap evolution under $\omega = 1.2$ rad/s

Case 7: Stable and overdamped condition in Region III

In this case, $\lambda_x = 0.8$ and $\lambda_v = 1.2$. We can derive that $\omega_0 = 0.8944$ rad/s and $\xi = 1.1180 > 1$, which means the platoon system is stable and overdamped. Figure 17-19 present the impact of a perturbation with various frequencies on the CAV platoon. These figures show a relatively mild oscillation. Among Figure 17-19, the perturbation with a resonance frequency in Figure 18 results in the largest oscillation. The amplitudes of velocity and space gap in Figure 18 are larger than those of other figures. Besides, because the vehicle platoon system is stable, all these figures present that perturbation decays as it propagates to the vehicle upstream.

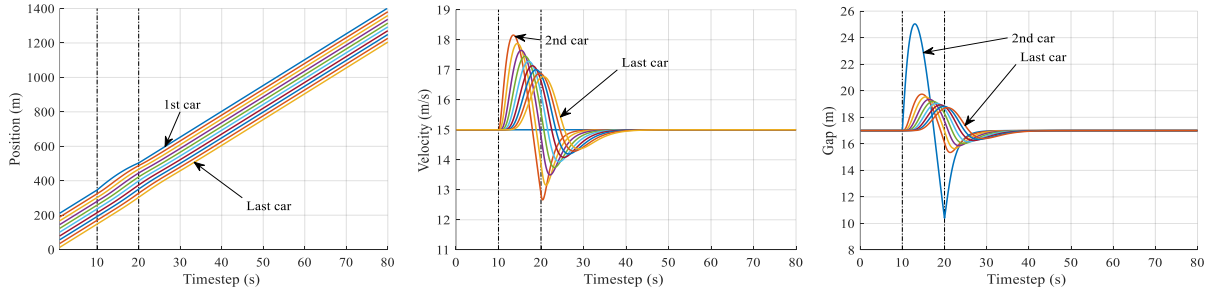

(a) Position vs. time (b) Velocity vs. time (a) Gap vs. time

Figure 17 Stable and overdamped platoon's position, velocity, and gap evolution under $\omega = 0.2$ rad/s

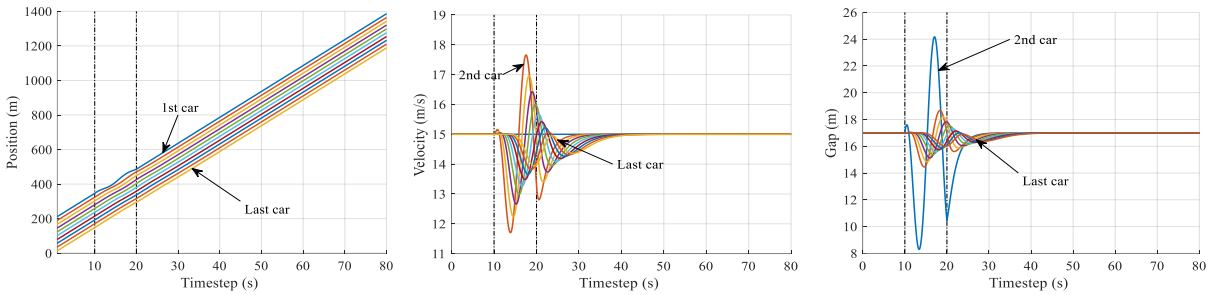

(a) Position vs. time (b) Velocity vs. time (a) Gap vs. time

Figure 18 Stable and overdamped platoon's position, velocity, and gap evolution under $\omega = \omega_0 = 0.8944$ rad/s

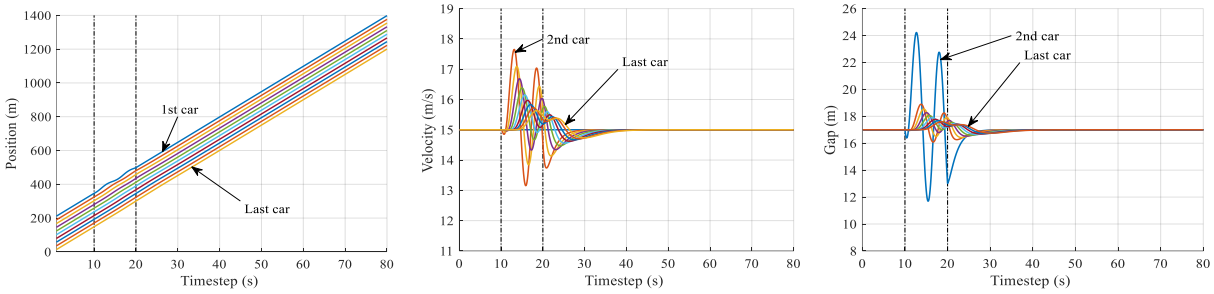

(a) Position vs. time (b) Velocity vs. time (a) Gap vs. time

Figure 19 Stable and overdamped platoon's position, velocity, and gap evolution under $\omega = 1.2$ rad/s

Case 8: Stable and underdamped condition in Region IV

In this case, we choose $\lambda_x = 0.8$ and $\lambda_v = 0.7$. Then we can compute $\omega_0 = 0.8944$ rad/s and $\xi = 0.8355 < 1$, which means the platoon system is stable and underdamped. The stable vehicle platoon system presents the magnitude of the perturbation damps out through the vehicle upstream. The underdamped system shows a back and force oscillation around the equilibrium state. Consistent with the above result, the oscillations of the vehicle platoon in Figure 21 are severest than the other two figures. This case also demonstrates that the perturbation with resonance frequency could cause the largest oscillatory amplitudes in velocity and space gap.

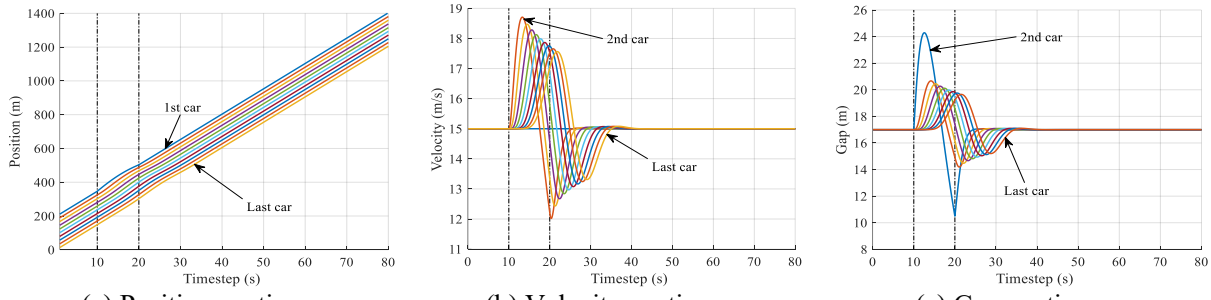

(a) Position vs. time (b) Velocity vs. time (a) Gap vs. time

Figure 20 Stable and underdamped platoon's position, velocity, and gap evolution under $\omega = 0.2$ rad/s

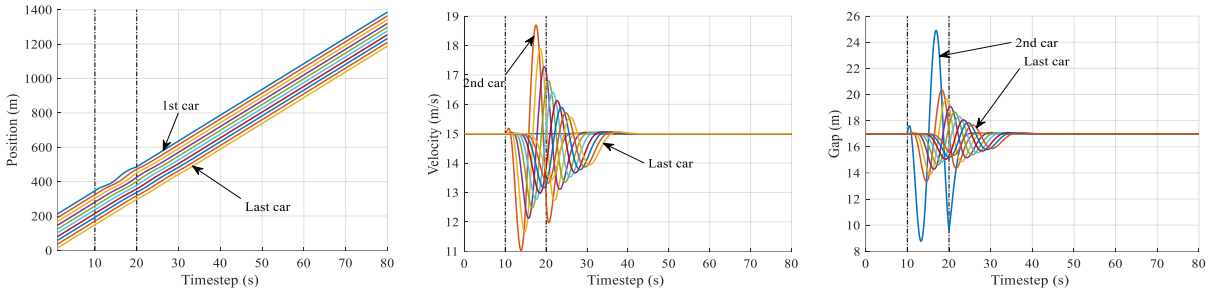

(a) Position vs. time (b) Velocity vs. time (a) Gap vs. time

Figure 21 Stable and underdamped platoon's position, velocity, and gap evolution under $\omega = \omega_0 = 0.8944$ rad/s

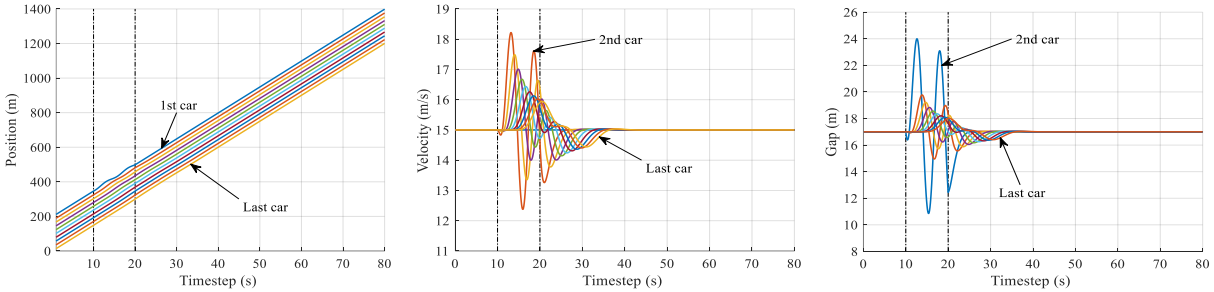

(a) Position vs. time (b) Velocity vs. time (a) Gap vs. time

Figure 22 Stable and underdamped platoon's position, velocity, and gap evolution under $\omega = 1.2$ rad/s

The simulation results show that different vehicle control parameters λ_x, λ_v could affect different oscillation patterns. The vehicle platoon presents a larger oscillation amplitude if the system is underdamped; otherwise, the vehicle platoon presents a smaller oscillation, and vehicles converge to a steady-state quickly. Meanwhile, these results also show that the periodic perturbations would lead to platoon oscillations and stop-and-go waves. Furthermore, among various periodic perturbations, the one with resonance frequency causes the severest oscillations and even rear-end collisions. This is also in line with the result of the mechanical vibration theory.

4.3 Scenario III: With human-driven vehicle trajectory from NGSIM

To analyze platoon oscillation in a more realistic situation, this scenario assumes that the first vehicle obeys a human-driven vehicle's trajectory from the NGSIM dataset (US Department of Transportation-FHWA, 2008). To date, the NGSIM data is the largest set of empirical microscopic traffic data available to the research community. Researchers have used these data to interpret traffic phenomena, support theories, benchmark, calibrate, and validate traffic flow

models (Montanino and Punzo, 2013; Zhou *et al.*, 2020). The NGSIM includes four data sets, *i.e.*, two from freeways (I-80 and US-101) and two from arterial corridors (Lankershim and Peachtree). Each data set includes complete vehicle trajectories for all vehicles over the freeway or arterial from the entrance to the exit.

In this scenario, we adopt the NGSIM trajectory data for I-80 in California to analyze the vehicle platoon's oscillation behaviors under different values of λ_x and λ_v. Same as Scenarios I and II, the vehicle platoon consists of ten vehicles, in which the first ~~leading~~ vehicle follows the human-driven vehicle's trajectory and the other nine CAVs obey the linear (Helly's) car-following model. Moreover, each CAV's car control parameters remain unchanged. Due to the noise in the trajectory data, we used the dataset filtered and reconstructed by (Montanino and Punzo, 2015) and (Punzo *et al.*, 2011). Without loss of generality, the first ~~leading~~ vehicle adopts the trajectory data of vehicle #1845 in the reconstructed NSGIM data, which is in Lane 2 from 4:00 p.m. to 4:15 p.m. on April 13, 2005. Figure 23 plots this vehicle's dynamic status.

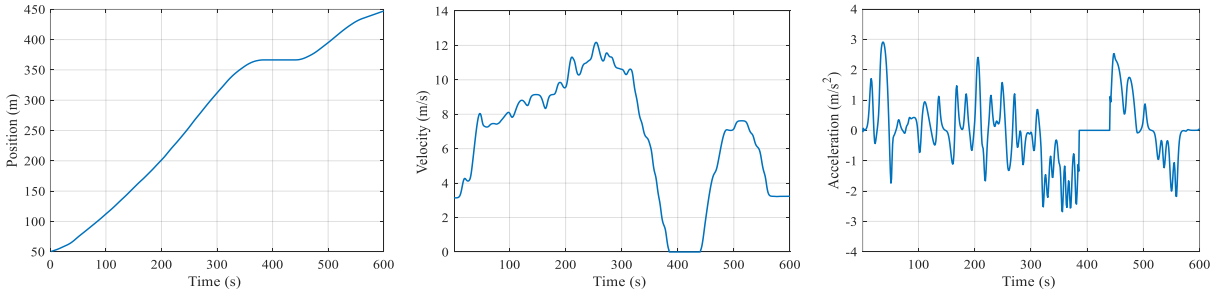

(a) Position vs. time (b) Velocity vs. time (c) Acceleration vs. time

Figure 23 Profiles of vehicle #1845 from I-80 data set (4:00-4:15 p.m.) of NGSIM data

Same as Scenarios I and II, we present four cases, corresponding to unstable and underdamped condition in Region I ($\lambda_x = 0.2$ and $\lambda_v = 0.3$), unstable and overdamped condition in Region II ($\lambda_x = 0.1$ and $\lambda_v = 0.7$), stable and overdamped condition in Region III ($\lambda_x = 0.8$ and $\lambda_v = 1.2$), and stable and underdamped condition in Region IV ($\lambda_x = 0.8$ and $\lambda_v = 0.7$), respectively. Most importantly, when the platoon system is unstable, the nine CAVs would cause rear-end collisions, as illustrated in Figure 24c and Figure 25c where the negative gaps represent collisions. By contrast, when the platoon system is stable, these vehicles do not collide, as illustrated in Figure 26c and Figure 27c. These results are in agreement with the theoretical results; namely, the perturbation effect decays for a stable system; otherwise, the perturbation effect grows for an unstable system (Pueboobpaphan and van Arem, 2010).

On the other hand, we can find that the underdamped system presents significantly back and forth oscillations, and the overdamped system presents slightly when comparing Figure 24 with

Figure 25 for unstable systems. In addition, the oscillation in the overdamped system decays over the vehicle platoon, while the oscillation in the underdamped system does not decay over the vehicle platoon when comparing Figure 26 with Figure 27 for stable systems.

This scenario also shows the complex platoon dynamics in a more realistic environment. In this scenario, parameters λ_x and λ_v selected from the unstable region could result in rear-end collisions. Furthermore, parameters λ_x and λ_v that make the vehicle platoon underdamped presents reciprocating oscillations.

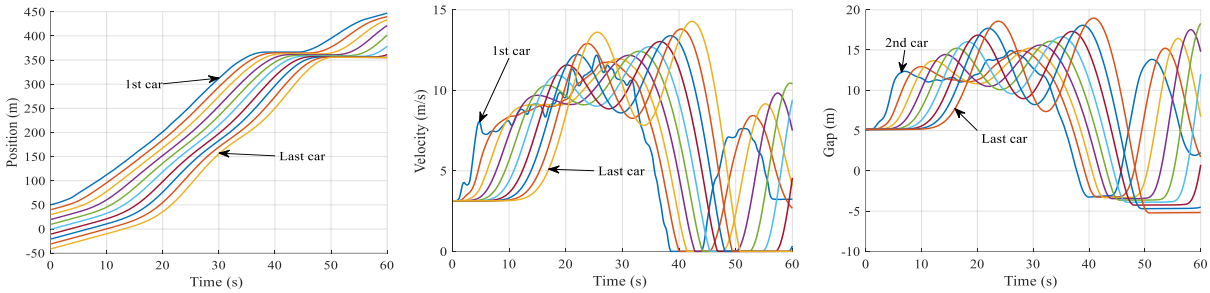

(a) Position vs. time (b) Velocity vs. time (c) Gap vs. time

Figure 24 Unstable and underdamped platoon's position, velocity, and gap evolution when $\lambda_x = 0.2$ and $\lambda_v = 0.3$

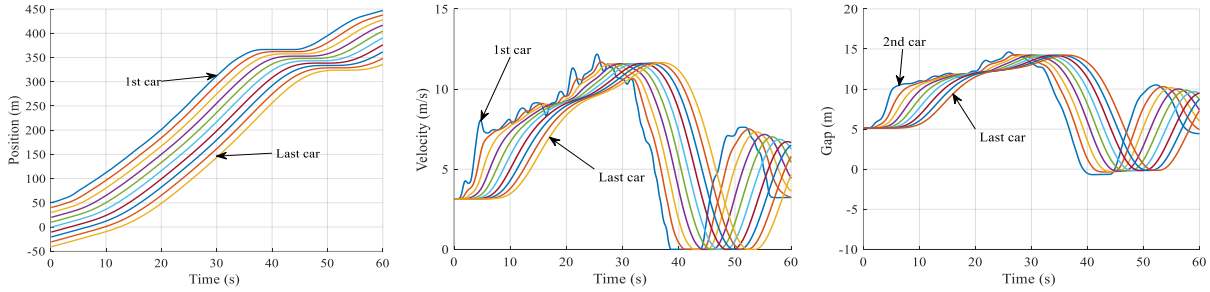

(a) Position vs. time (b) Velocity vs. time (c) Gap vs. time

Figure 25 Unstable and overdamped platoon's position, velocity, and gap evolution when $\lambda_x = 0.1$ and $\lambda_v = 0.7$

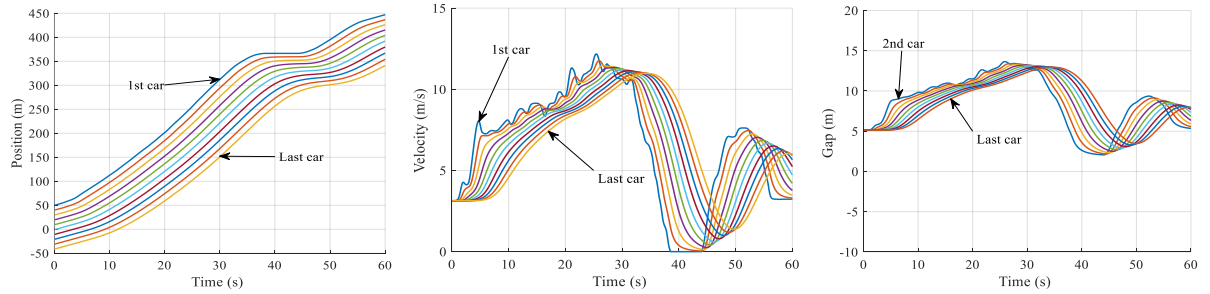

(a) Position vs. time (b) Velocity vs. time (c) Gap vs. time

Figure 26 Stable and overdamped platoon's position, velocity, and gap evolution when $\lambda_x = 0.8$ and $\lambda_v = 1.2$

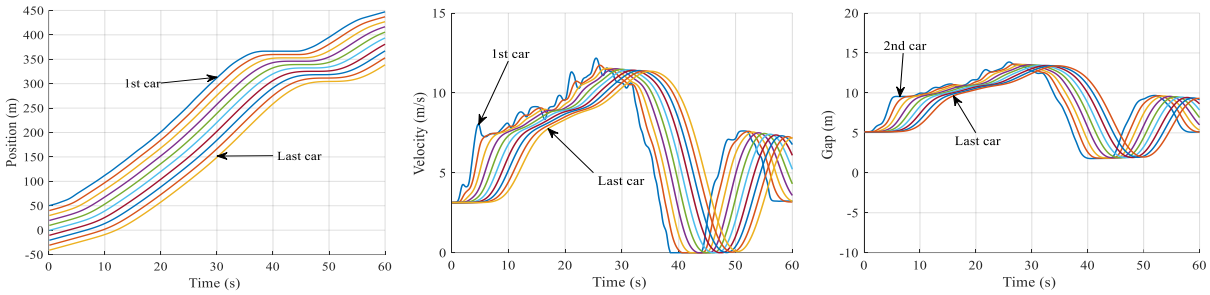

(a) Position vs. time (b) Velocity vs. time (c) Gap vs. time

Figure 27 Stable and underdamped platoon's position, velocity, and gap evolution when $\lambda_x = 0.8$ and $\lambda_v = 0.7$

Through all three scenarios, we demonstrate how parameters λ_x and λ_v characterize the system's oscillations in addition to their impact on system stability. Some common features have been illustrated. For instance, ~~the unstable platoon system shows a larger oscillation than the stable system. Even worse, the unstable platoon system with particular settings could result in collisions. On the other hand,~~ the overdamped platoon system hardly oscillates, and the underdamped platoon system oscillates back and forth. Furthermore, these scenarios show unique results. For example, Scenario I presents that the larger the value of the damping intensity ξ for the platoon system, the smaller the oscillation behaviors of the platoon. Scenario II shows that, among various periodic perturbations, the one with resonance frequency causes the severest oscillations and even rear-end collisions. And Scenario III shows that our proposed approach is effective to analyze vehicle platoon damping behavior in a more realistic travel environment. ~~which presents for the unstable platoon, an accident happens; for the stable system, the oscillation in the (over)underdamped system (does not)decays over the vehicle platoon.~~ These scenarios help deepen our understanding of platoon systems' damping behavior and stability.

5. Conclusions

This research presents the damping-based oscillation analysis and illustrates the differences between oscillation and instability. The instability is used to decide whether the vehicle platoon system is stable or unstable. In contrast, the damping-based oscillation analysis reveals the inherent characteristics of platoon oscillation. In this study, to better derive the damping oscillation characteristics, a classic linear car-following model, Helly's model, is adopted and reformulated as a mathematical representation of the mechanical vibration based on the similarity between mechanical vibrations and platoon oscillations. The theoretical results reveal that the oscillation of a CAV platoon is mainly associated with its resonance frequency, through

which a small perturbation can amplify its effect to increase the platoon oscillation amplitude. The paper demonstrates that resonance could lead to the severest oscillations among various periodic perturbation frequencies through simulation. As a result, protecting the platoon from resonance is crucial to enhance the CAV platooning reliability and suppress large amplitude oscillations. These results also demonstrate the effectiveness of our proposed approach to characterize the damping oscillation properties of the CAV platoon and the importance of analyzing platoon oscillation behavior.

The current research can be further extended in several directions. First, the derived damping conditions only focus on the linear car-following model. It will be interesting to investigate the oscillation frequency and damping parameter for nonlinear car-following models, such as the Intelligent Driver Model. Also, the theoretical derivation for the vehicle platoon with the simple communication scheme ignores the communication attributes, such as communication topology and delay, which affect the platoon stability as proved in the literature. Third, this study adopts a classical frequency-domain method to demonstrate the differences between the string stability and the proposed vulnerability analysis approach. Other stability analysis methods, such as L_2 and L_∞, and their differences to our proposed approach, are worth further investigation.

Acknowledgments

This work was supported in part by the Young Scientists Fund of the National Natural Science Foundation of China (52002013), China Postdoctoral Science Foundation (BX20200036, 2020M680298), and the U.S. National Science Foundation via Grant CMMI-2047793. The authors are solely responsible for the contents of this paper.

APPENDIX

This study adopts the linear stability analysis method (Bando *et al.*, 1995; Kesting and Treiber, 2013; Ngoduy, 2015; Wilson, 2008) to analyze the (in)stability of Helly's model. When the velocity deviation μ_n and a space gap deviation y_n are small enough, employing the first-order Taylor expression, Eq. (7) can be rewritten as

$$\dot{\mu}_n = f_n^v \mu_n + f_n^s y_n + f_n^{\Delta v} \Delta\mu_n, \tag{20}$$

where $f_n^v = \left.\frac{\partial f}{\partial v_n}\right|_{(v^e, s^e, 0)}$, $f_n^s = \left.\frac{\partial f}{\partial s_n}\right|_{(v^e, s^e, 0)}$ and $f_n^{\Delta v} = \left.\frac{\partial f}{\partial \Delta v_n}\right|_{(v^e, s^e, 0)}$.

The velocity deviation μ_n and the space gap deviation y_n are set as two exponential functions $\mu_n = Ae^{i\omega n+\lambda t}$ and $y_n = Be^{i\omega n+\lambda t}$, in which A, B are constant. A prevailing reason is that their *k*-th derivations are proportional to these functions themselves.

Given that $\dot{s}_n = v_{n-1} - v_n$, we have

$$B = \frac{A(e^{-i\omega} - 1)}{\lambda}. \tag{21}$$

Submitting Eq. (21) into Eq. (20), we can derive the characteristic equation as below.

$$\lambda^2 - \lambda\left(f_n^v + f_n^{\Delta v}(1 - e^{-i\omega})\right) - \left(e^{-i\omega} - 1\right) f_n^s = 0. \tag{22}$$

Extending λ in a power series solution $\lambda = i\omega\lambda_1 + \omega^2\lambda_2 + o(\omega)$, where λ_1 and λ_2 are real coefficients. Then submitting it into Eq. (22), we have

$$\begin{aligned} \lambda_1 &= \frac{f_n^s}{f_n^v}, \\ \lambda_2 &= -\frac{(f_n^s)^2}{(f_n^v)^3} + \frac{f_n^s f_n^{\Delta v}}{(f_n^v)^2} + \frac{f_n^s}{2f_n^v}. \end{aligned} \tag{23}$$

The platoon is linearly stable if $\lambda_2 \le 0$. These partial differential equations in Eq. (23) satisfy the following conditions,

$$f_n^v \le 0,\ f_n^s \ge 0,\ f_n^{\Delta v} \le 0. \tag{24}$$

In fact, Eq.(24) presents a practical meaning. In a close-following situation, a larger space gap would lead to the following vehicle's more acceleration since the preceding vehicle is leaving away; a larger velocity difference would lead to more deceleration due to the fact that the following vehicle is quickly close to the vehicle ahead; the larger its own velocity, its deceleration tendency accelerate would be more. In particular, $f_n^s = 0$ and $f_n^{\Delta v} = 0$ mean that no following relationship between two successive vehicles (Wilson and Ward, 2011).

Hence, we can derive the stable condition as follows.

$$-\frac{f_n^s}{f_n^v} + f_n^{\Delta v} + \frac{f_n^v}{2} \le 0. \tag{25}$$

Similarly, the unstable condition is obtained, *i.e.*,

$$-\frac{f_n^s}{f_n^v} + f_n^{\Delta v} + \frac{f_n^v}{2} > 0. \tag{26}$$

Furthermore, we can get the analytic expressions of partial differential equations of Helly's model:

$$f_n^v = -\lambda_x\tau,\ f_n^s = \lambda_x,\ f_n^{\Delta v} = -\lambda_v. \tag{27}$$

Then applying the instability criteria Eq. (26) to Helly's model, we can get its instability condition, *i.e.*,

$$\lambda_v < \frac{1}{\tau} - \frac{\lambda_x \tau}{2}. \tag{28}$$

References

Aghabayk, K., Sarvi, M., Young, W., 2015. A state-of-the-art review of car-following models with particular considerations of heavy vehicles. Transport Reviews 35 (1), 82-105.

Ahn, S., Cassidy, M.J., 2007. Freeway traffic oscillations and vehicle lane-change maneuvers. In: The 17th International Symposium on Transportation and Traffic Theory (ISTTT17), London, UK, 691-710.

Bando, M., Hasebe, K., Nakayama, A., Shibata, A., Sugiyama, Y., 1995. Dynamical model of traffic congestion and numerical simulation. Physical Review E 51 (2), 1035-1045.

Bang, S., Ahn, S., 2020. Analysis and control of heterogeneous connected and autonomous vehicles using a spring-mass-damper system. Transport. Res. Rec. 2674 (8), 309-318.

Chandler, R.E., Herman, R., Montroll, E.W., 1958. Traffic dynamics: Studies in Car Following. Oper. Res. 6 (2), 165-184.

Chen, N., van Arem, B., Alkim, T., Wang, M., 2021. A hierarchical model-based optimization control approach for cooperative merging by connected automated vehicles. IEEE T. Intell. Transp. 22 (12), 7712-7725.

Daganzo, C.F., Gayah, V.V., Gonzales, E.J., 2011. Macroscopic relations of urban traffic variables: Bifurcations, multivaluedness and instability. Transportation Research Part B: Methodological 45 (1), 278-288.

Ding, F., Jiang, J., Zhou, Y., Yi, R., Tan, H., 2020. Unravelling the impacts of parameters on surrogate safety measures for a mixed platoon. Sustainability-Basel 12 (23), 9955.

Dong, J., Chen, S., Li, Y., Du, R., Steinfeld, A., Labi, S., 2021. Space-weighted information fusion using deep reinforcement learning: The context of tactical control of lane-changing autonomous vehicles and connectivity range assessment. Transportation Research Part C: Emerging Technologies 128, 103192.

Hahn, L., 1994. Complex numbers and geometry. Cambridge University Press.

Helly, W., 1959. Simulation of bottlenecks in single-lane traffic flow. In: Proceedings of the Symposium on theory of traffic flow, New York, 207-238.

Herman, I., Martinec, D., Hurák, Z., Šebek, M., 2015. Nonzero bound on fiedler eigenvalue causes exponential growth of H-Infinity Norm of vehicular platoon. IEEE T. Automat. Contr. 60 (8), 2248-2253.

Herman, R., Montroll, E.W., Potts, R.B., Rothery, R.W., 1959. Traffic dynamics: analysis of stability in car following. Oper. Res. 7 (1), 86-106.

Horn, B.K., Wang, L., 2018. Wave equation of suppressed traffic flow instabilities. IEEE T. Intell. Transp. 9 (19), 2955-2964.

Hu, Y., Ma, T., Chen, J., 2021. Multi-anticipative bi-directional visual field traffic flow models in the connected vehicle environment. Physica A: Statistical Mechanics and its Applications 584, 126372.

Jia, D., Ngoduy, D., 2016. Platoon based cooperative driving model with consideration of realistic inter-vehicle communication. Transportation Research Part C: Emerging Technologies 68, 245-264.

Jiang, R., Jin, C., Zhang, H.M., Huang, Y., Tian, J., Wang, W., Hu, M., Wang, H., Jia, B., 2018. Experimental and empirical investigations of traffic flow instability. Transportation Research Part C: Emerging Technologies 94, 83-98.

Kelly, S.G., 2012. Mechanical vibrations: theory and applications. Cengage Learning, Stamford, CT, USA.

Kesting, A., Treiber, M., 2013. Traffic Flow Dynamics: Data, Models and Simulation. Springer, Berlin.

Li, X., Peng, F., Ouyang, Y., 2010. Measurement and estimation of traffic oscillation properties. Transportation Research Part B: Methodological 44 (1), 1-14.

Li, Y., Chen, W., Peeta, S., He, X., Zheng, T., Feng, H., 2017. An extended microscopic traffic flow model based on the spring-mass system theory. Mod. Phys. Lett. B 31 (9), 1750090.

Li, Z., Khasawneh, F., Yin, X., Li, A., Song, Z., 2020. A New Microscopic Traffic Model Using a Spring-Mass-Damper-Clutch System. IEEE T. Intell. Transp. 21 (8), 3322-3331.

Milanes, V., Shladover, S., 2014. Modeling cooperative and autonomous adaptive cruise control dynamic responses using experimental data. Transportation Research Part C: Emerging Technologies 48, 285-300.

Montanino, M., Punzo, V., 2013. Making NGSIM Data Usable for Studies on Traffic Flow Theory:Multistep Method for Vehicle Trajectory Reconstruction. Transport. Res. Rec. 2390 (1), 99-111.

Montanino, M., Punzo, V., 2015. Trajectory data reconstruction and simulation-based validation against macroscopic traffic patterns. Transportation Research Part B: Methodological 80, 82-106.

Montanino, M., Punzo, V., 2021. On string stability of a mixed and heterogeneous traffic flow: A unifying modelling framework. Transportation Research Part B: Methodological 144, 133-154.

Munigety, C.R., 2018. A spring-mass-damper system dynamics-based driver-vehicle integrated model for representing heterogeneous traffic. Int. J. Mod. Phys. B 32 (11), 1850135.
Naus, G.J., Vugts, R.P., Ploeg, J., van de Molengraft, M.J., Steinbuch, M., 2010. String-stable CACC design and experimental validation: A frequency-domain approach. IEEE T. Veh. Technol. 59 (9), 4268-4279.
Ngoduy, D., 2013. Instability of cooperative adaptive cruise control traffic flow: A macroscopic approach. Commun. Nonlinear Sci. 18 (10), 2838-2851.
Ngoduy, D., 2015. Linear stability of a generalized multi-anticipative car following model with time delays. Commun. Nonlinear Sci. 22 (1-3), 420-426.
Niroumand, R., Tajalli, M., Hajibabai, L., Hajbabaie, A., 2020. Joint optimization of vehicle-group trajectory and signal timing: Introducing the white phase for mixed-autonomy traffic stream. Transportation Research Part C: Emerging Technologies 116, 102659.
Norton, M.P., Karczub, D.G., 2003. Fundamentals of noise and vibration analysis for engineers. Cambridge University Press.
Papadoulis, A., Quddus, M., Imprialou, M., 2019. Evaluating the safety impact of connected and autonomous vehicles on motorways. Accident Analysis & Prevention 124, 12-22.
Ploeg, J., Van De Wouw, N., Nijmeijer, H., 2014. Lp string stability of cascaded systems: Application to vehicle platooning. IEEE T. Contr. Syst. T. 22 (2), 786-793.
Pueboobpaphan, R., van Arem, B., 2010. Understanding the relation between driver and vehicle characteristics and platoon and traffic flow stability for the design and assessment of cooperative adaptive cruise control. Transport. Res. Rec. (2189), 88-97.
Punzo, V., Borzacchiello, M.T., Ciuffo, B., 2011. On the assessment of vehicle trajectory data accuracy and application to the Next Generation SIMulation (NGSIM) program data. Transportation Research Part C: Emerging Technologies 19 (6), 1243-1262.
Qin, Y., Li, S., 2020. String stability analysis of mixed CACC vehicular flow with vehicle-to-vehicle communication. IEEE Access 8, 174132-174141.
Saxena, N., Rashidi, T.H., Dixit, V.V., Waller, S.T., 2019. Modelling the route choice behaviour under stop-&-go traffic for different car driver segments. Transportation Research Part A: Policy and Practice 119, 62-72.
Schmitz, T.L., Smith, K.S., 2011. Mechanical vibrations: modeling and measurement. Springer Science & Business Media, New York, NY.
Shabana, A.A., 2019. Theory of vibration: An introduction. Springer, Chicago, IL, USA.
Shladover, S.E., 2018. Connected and automated vehicle systems: Introduction and overview. J. Intell. Transport. S. 22 (3), 190-200.
Sun, J., Zheng, Z., Sun, J., 2018. Stability analysis methods and their applicability to car-following models in conventional and connected environments. Transportation Research Part B: Methodological 109, 212-237.
Swaroop, D., Hedrick, J.K., 1996. String stability of interconnected systems. IEEE T. Automat. Contr. 41 (3), 349-357.
Thomson, W., 2018. Theory of vibration with applications. CRC Press, Boca Raton, FL, USA.
Treiber, M., Kesting, A., 2018. The Intelligent Driver Model with stochasticity - New insights into traffic flow oscillations. Transportation Research Part B: Methodological 117, 613-623.
US Department of Transportation-FHWA, 2008. NGSIM-Next Generation SIMulation. <https://ops.fhwa.dot.gov>.
Vegamoor, V., Rathinam, S., Darbha, S., 2021. String stability of connected vehicle platoons under lossy V2V communication. IEEE T. Intell. Transp., doi: 10.1109/TITS.2021.3086809.
Wang, P., Wu, X., He, X., 2020. Modeling and analyzing cyberattack effects on connected automated vehicular platoons. Transportation Research Part C: Emerging Technologies 115, 102625.
Wang, Z., Bian, Y., Shladover, S.E., Wu, G., Li, S.E., Barth, M.J., 2019. A survey on cooperative longitudinal motion control of multiple connected and automated vehicles. IEEE Intelligent Transportation Systems Magazine 12 (1), 4-24.
Wilson, R.E., 2008. Mechanisms for spatio-temporal pattern formation in highway traffic models. Philosophical Transactions of the Royal Society of London A: Mathematical, Physical and Engineering Sciences 366 (1872), 2017-2032.
Wilson, R.E., Ward, J.A., 2011. Car-following models: fifty years of linear stability analysis-a mathematical perspective. Transport. Plan. Techn. 34 (1), 3-18.
Xiao, L., Gao, F., 2011. Practical string stability of platoon of adaptive cruise control vehicles. IEEE T. Intell. Transp. 12 (4), 1184-1194.
Yanakiev, D., Kanellakopoulos, I., 1996. A simplified framework for string stability analysis in AHS. IFAC Proceedings Volumes 29 (1), 7873-7878.
Yao, H., Li, Q., Li, X., 2020. A study of relationships in traffic oscillation features based on field experiments. Transportation Research Part A: Policy and practice 141, 339-355.
Zhou, Y., Ahn, S., Wang, M., Hoogendoorn, S., 2020. Stabilizing mixed vehicular platoons with connected

automated vehicles: An H-infinity approach. Transportation Research Part B: Methodological 132, 152-170.
Zhou, Y., Wang, M., Ahn, S., 2019. Distributed model predictive control approach for cooperative car-following with guaranteed local and string stability. Transportation Research Part B: Methodological 128, 69-86.